I&EC research
Industrial & Engineering Chemistry Research

Applied Chemistry

A Combined Experimental and Computational Study of Polyaromatic Hydrocarbon Aggregation – Isolating the Effect of Attached Functional Groups

Dorin Simionesie, Gregory O'Callaghan, Raphael Laurent, Jon A. Preece, Robert Evans, and Zhenyu J. Zhang

Ind. Eng. Chem. Res., **Just Accepted Manuscript** • DOI: 10.1021/acs.iecr.9b04105 • Publication Date (Web): 22 Oct 2019

A Combined Experimental and Computational Study of Polyaromatic Hydrocarbon Aggregation – Isolating the Effect of Attached Functional Groups

Dorin Simionesie, [†] *Gregory O'Callaghan,*[‡] *Raphael Laurent,*[§] *Jon A. Preece,*[‡] *Robert Evans,*[§]* *and Zhenyu J. Zhang*[†]*

[†]School of Chemical Engineering, University of Birmingham, Edgbaston, Birmingham, B15 2TT, U.K.

[‡]School of Chemistry, University of Birmingham, Edgbaston, Birmingham, B15 2TT, U.K.

[§]Aston Institute of Materials Research, School of Engineering and Applied Science, Aston University, Birmingham, B4 7ET, U.K.

ABSTRACT

To establish, and isolate, the influence of different chemical functional groups on the aggregation of polyaromatic hydrocarbons, a series of triphenylene-based compounds were investigated using experimental and computational approaches together. Containing alkoxy- side chains of varying length and amide appendages, both with and without a terminating carboxylic acid, their aggregation structures, sizes, and kinetics in toluene were studied over several length scales, using a combination of Dynamic Light Scattering (DLS) and Diffusion-Ordered NMR spectroscopy (DOSY), complemented with Molecular Dynamics (MD) simulations. There is a strong correlation between molecular architecture and aggregation mechanisms across different length scales: addition of polar functional groups and heteroatoms resulted in compounds that are more prone to aggregation and form large, micrometer-sized clusters, while the increased steric hindrance imposed by alkoxy- side chains led to stable nanometer-sized aggregates. These conclusions underline the strong structure-function relationship of polyaromatic hydrocarbons, such as asphaltenes, examined here over multiple size-scales in a single solvent. We also demonstrated the importance of using complementary techniques to study the aggregation process of polyaromatic hydrocarbons that could form aggregates of various sizes over different timescales.

INTRODUCTION

Aggregation of polyaromatic hydrocarbons (PAHs), in particularly natural asphaltenes, has attracted extensive research efforts from both academia and industry for decades.[1-6] The definition of asphaltene, which is arguably over-simplified, is the fraction of crude oil that is soluble in aromatic solvent such as toluene and benzene, but insoluble in *n*-heptane. Understanding the mechanism by which such aggregation occurs, at what level (molecular or colloidal), in what environment, and the functional groups that drive the process is critical for developing strategies in mitigating such issues that cause industry billions of dollars per year.[8]

Recent investigations of both "archipelago"[11] and "continental" models of asphaltenes[12] suggest that they associate and form nanoaggregates in toluene, driven primarily by π-π stacking interactions between the aromatic rings.[6, 12,13] In turn, nanoaggregates associate and form larger macroaggregates. It has been recognised that the presence of side groups promotes asphaltenes to aggregate into stacks in both continuous oil phases and at oil-water interfaces.[14-17] Different chain lengths of side groups influence the interactions between the asphaltene molecules, and modulate any aggregation.[18]

Previous studies illustrate two key aspects of PAHs aggregation. First, that aggregation typically occurs over two important length scales. The molecules initially form nanoaggregates, comprising of a few molecules, and stay dispersed. They can, however, quickly aggregate into larger macroaggregates once being destabilized. Any experimental measurements of aggregation process need to survey both type of aggregate. Second, the range of chemical moieties that can be incorporated into PAHs is vast, including heteroatoms (N, S, and O), functional groups such as amides and carboxylic acids, and even metals (Ni and V), in addition to one or more aromatic core with alkyl side chains. Any attempt to understand the mechanism by which asphaltene aggregation occurs and isolate the functional groups that drive the process needs to take both aspects into account.

To isolate the roles of different functional groups and identify the dominant driving forces of the aggregation, seven model molecules have been developed to study the underpinning mechanisms.[11,22,23] This set of PAHs are all based on a central triphenylene core with both symmetrically- and asymmetrically-arranged alkyl chains, as well as functional groups such as amides and acids, as substituents. Acid groups have previously been attached to triphenylene with the purpose of controlling the properties (such as thermal stability) of the structures formed, and have proved to enhance the intermolecular interactions, by increasing the polarity of the compounds.[29] The increase in the number of active aggregation sites, such as heteroatoms and functional groups, per molecule as has been shown to increase the aggregation potential of the compounds studied.[30-35]

Dynamic light scattering (DLS) was used to study the aggregates of triphenylene derivatives in toluene. Although previous DLS studies of model asphaltenes succeeded in identifying critical concentrations, solvent reactivity, and the impact of functional group percentages on the aggregation of asphaltenes,[36,37] the results are usually highly dependent on the exact nature of the samples,[38,39] from which a generic mechanism is hard to conclude. Diffusion nuclear magnetic resonance (NMR) technique, also known as diffusion-ordered spectroscopy (DOSY),[40,41] is another technique previously used to study asphaltenes aggregation.[42-48] The diffusion coefficients of signals originating from different species are separated in a 2-dimensional NMR spectrum, allowing for the identification of different species in the sample on the basis of both chemistry and size.

The experimental methods are complemented by Molecular Dynamics (MD) simulations where chemical structures of the same compounds are constructed and dispersed in toluene to investigate the intermolecular interactions.[49] In addition to the graphical description, radial distribution functions (RDFs) are used to evaluate the packing distances and configurations of asphaltene model compounds as a function of solvent species,[50] and intermolecular distances. The advantage of our approach is that the complementary experimental techniques, DLS and diffusion NMR spectroscopy, characterise the size and stability of the aggregates formed from nano- to microscales, whilst MD simulations are used to give molecular insight into the aggregation and stabilization mechanisms. A consistent set of model compounds allows for the role of different functional groups and differently sized alkyl chains to be isolated and their effects on aggregation identified.

MATERIALS AND METHODS

Materials

Toluene of different grades (99.85 %, Extra Dry–AcroSeal; 99+ %, extra pure and deuterated (d_8)) and PTFE membrane filters (100 nm pore size, Whatman) were purchased from Fisher Scientific (Loughborough, UK). Quartz optical cell (S High Precision Cell – light path 3×3 mm) was purchased from Hellman Analytics Q.

The chemical structures of model compounds studied are presented in Figure 1. Corresponding information, including name of the model compounds, relative molar mass (RMM), hydrogen to carbon ratio (H/C), and oxygen to carbon ratio (O/C), is presented in Table 1. TPN-C0 (triphenylene) was purchased from Sigma Aldrich (Dorset, UK). The other model compounds were prepared by the procedures detailed in the Supporting Information.[51]

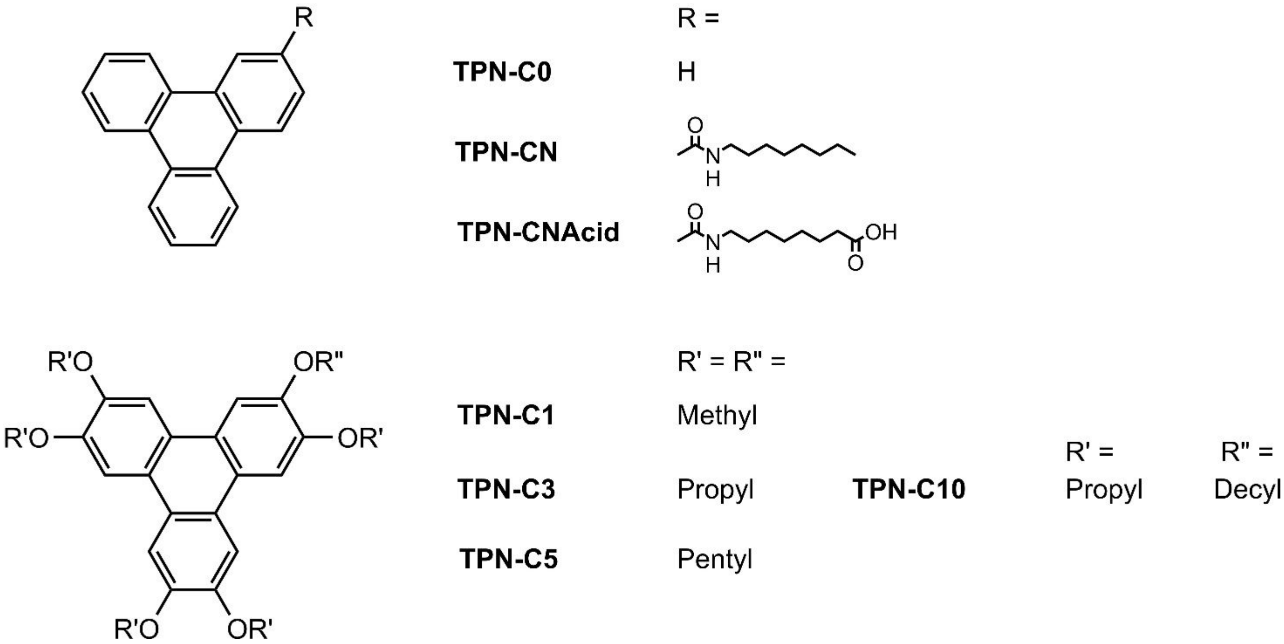

Figure 1. Chemical structures of the seven triphenylene derivatives used in the present study.

Model compound	RMM / g mol^{-1}	H/C Ratio / %	O/C Ratio / %
TPN-C0	228.09	5.6	0.0
TPN-CN	383.22	9.0	4.9
TPN-CNAcid	413.22	8.4	14.8
TPN-C1	408.16	8.4	33.3
TPN-C3	576.35	11.2	22.2
TPN-C5	744.53	12.6	16.6
TPN-C10	674.45	12.1	18.6

Table 1. Table of RMM, H/C and C/O ratio data for the seven triphenylene derivatives used in the present study

Methods

Dynamic light scattering

Solutions/dispersions of the model compounds were kept at 22 ± 0.5°C and ambient pressure, with minimal exposure to visible light. All solvents were filtered three times with PTFE filters (100 nm pore size) prior to usage. DLS measurements were carried out using a Zetasizer (Malvern, UK) (λ = 632.8 nm, scattering angle 173°), with data acquisition at 0, 24, 168 hours. Data analysis was performed using the integrated software. Each datum is an averaged value of three samples, each measured over six repeats. The mean diffusivity, D, of aggregates was calculated based on the initial decay rate of the normalised intensity autocorrelation function acquired, $g_2(\tau)$, using Eq. 1:

$$g_2(\tau) = e^{-2Dq\tau} \tag{1}$$

where τ is the delay time and q is the scattering wave vector magnitude,

$$q = \frac{4\pi n}{\lambda} sin\left(\frac{\theta}{2}\right) \tag{2}$$

where n is the refractive index of the solvent, λ is the wavelength of the laser and θ is the scattering angle. Stokes-Einstein equation (Eq. 3) was subsequently used to calculate the hydrodynamic radius of the aggregate, r_H

$$r_\mathrm{H} = \frac{kT}{6\pi\eta D} \tag{3}$$

where k is Boltzmann's constant, T is the absolute temperature, and η is the viscosity of the solvent.[52,53] All model compounds were measured at 10 mg/mL.

Diffusion NMR

Solutions of each model compounds with nominal concentrations of 10 mg/mL were prepared in toluene-d_8, with tetramethylsilane added as a reference (both Sigma Aldrich (Dorset, UK)). All measurements were carried out, non-spinning, on a 300 MHz Bruker Avance spectrometer, using a 5 mm PABBO BB-1H ZGRD probe equipped with a z gradient coil producing a maximum gradient of 36 G cm^{-1}. All NMR measurements were made at 22 ± 0.5°C. DOSY spectra were constructed in the DOSY Toolbox[54] by fitting to a modified Stejskal Tanner equation, and diffusion coefficients were obtained from the statistics of the fit. Further details on diffusion NMR methodology can be found in the Supporting Information.[55]

A typical DOSY spectrum, showing data acquired for TPN-C3, is presented in Figure 2. The horizontal axis is a standard 1D ^{1}H spectrum, with the diffusion information contained in the vertical axis. Signals originating from any one molecule will all have the same diffusion coefficient and be found on the same horizontal line, as observed in Figure 3 for all three species in the sample; TPN-C3, solvent and reference material. All DOSY spectra used in this study can be found in Supporting Information.

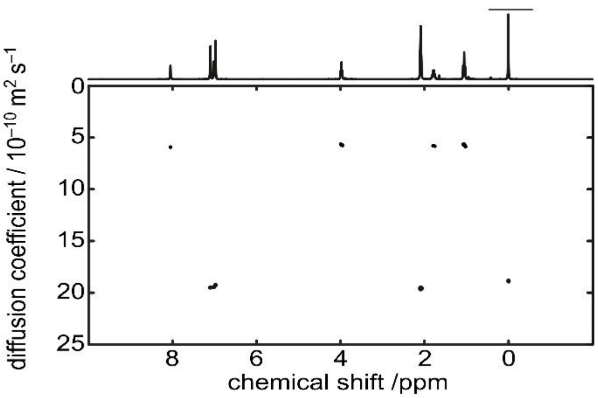

Figure 2. Representative DOSY spectrum of TPN-C3 in toluene-d_8. All experimental details of diffusion NMR study are included in the Supplementary Information.

Diffusion coefficients estimated from DOSY spectra are related to hydrodynamic sizes through the Gierer-Wirtz (G-W or SEGWE) modification of the Stokes-Einstein equation (Eqn. 4).[56-59] This approach, where α is the ratio of solvent molecular weight to solute molecular weight, is more accurate for smaller species.

$$D = \frac{kT}{6\pi\eta r_{\mathrm{H}}} \cdot \left(\frac{3\alpha}{2} + \frac{1}{1+\alpha}\right) \tag{4}$$

By combining the Gierer-Wirtz modification with appropriate assumptions about factors such as solute shape, flexibility, and solvation, the expected diffusion coefficients of molecules, based on their molecular weight, can also be estimated.

Molecular dynamics simulation

Molecular dynamics simulations were carried out using a GROMACS 4.6.5 software package.[12,60,61] An OPLS/AA force field was chosen as it has been tested previously with polyaromatic molecules,[62] and has been proven to be reliable in examining compounds similar to those studied in this work.[63,64] Models of each synthesized polyaromatic model compound were constructed based on protocols established in a previous study.[65] Seven identical molecules of each compound were placed in a toluene simulation box (700 toluene molecules) at equal distant positions to examine the intermolecular forces between the model compounds in toluene. The dimension of the simulation box is fixed at 5 nm (± 0.3 nm) in each direction, constraining the maximum distance between each pair of molecules. All simulations were performed for 100 ns.

Following the simulations, radial distribution functions were produced for all chemicals examined, where the height of the peaks (intensity of G(r)) indicates the density of the interaction between the model compounds, whilst the position of the peak shows intermolecular distances. The RDFs for all compounds were normalized by the value of the highest datum of all model compounds. Second, the distances between the centers of mass (COM) of the molecules in the simulation box can be plotted. This gives information about pairs, triplets or larger numbers of molecules that have clustered together at a fixed distance from one another.

RESULTS

Dynamic light scattering of model compounds

The hydrodynamic diameters of aggregates in toluene were measured as a function of time for all seven model compounds using dynamic light scattering at an angle of 173°. The averaged hydrodynamic diameters acquired, with corresponding standard errors, are presented in Figure 3. The data collected reveals not only the effect of the peripheral aliphatic chain length and functional groups on aggregation, but also the corresponding kinetics.

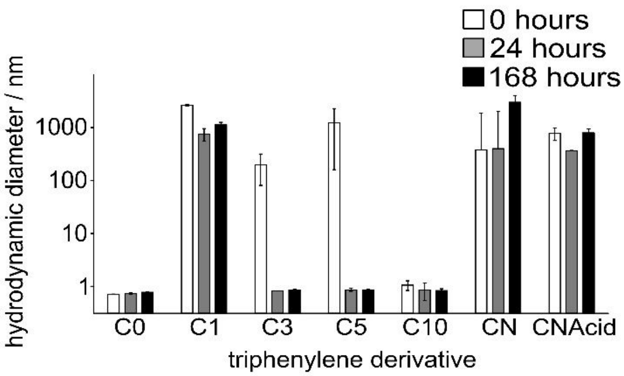

Figure 3. Averaged hydrodynamic diameters for all seven model PAH compounds at 10 mg/mL, acquired using dynamic light scattering at an angle of 173°, in toluene at 0 (white), 24 (grey), and 168 hours (black) after sample preparation.

The benchmark PAH, TPN-C0, was found to disperse fully in toluene, resulting in an initial hydrodynamic diameter under 1 nm, consistent with the hydrodynamic diameter of an individual triphenylene molecule. This hydrodynamic diameter remains constant throughout the measurement period. The compounds with an additional 6 alkoxy side chains, symmetrically arranged around the polyaromatic core, TPN-C1, TPN-C3, and TPN-C5, were found to form large aggregates (>100 nm) initially in toluene, which suggests that alkyl side chains readily facilitate aggregation. However, such an effect is not applicable with TPN-C10 that has an initial hydrodynamic diameter comparable to TPN-C0, implying an immediate dissolution. After 24 hours, there was a significant reduction in hydrodynamic diameters for TPN-C3 and TPN-C5, with final sizes similar to that observed for TPN-C0. These two PAHs could dissociate substantially from their initial aggregating configurations.

However, TPN-C1, possessing only short methoxy- chains, did not significantly dissociate and the hydrodynamic radius remained at *ca*. 1000 nm.

TPN-CN and TPN-CNAcid formed large aggregates initially, with sizes ~400 nm and ~800 nm respectively. After 24 hours, the size of the TPN-CN aggregates remained broadly constant (~400 nm), whilst that of TPN-CNAcid aggregates was reduced to nearly half of the initial value. The hydrodynamic diameters of both TPN-CN and TPN-CNAcid increased to ~3000 nm and ~800 nm respectively after 168 hours. It is very probable that these size variations observed are due to continuous re-configurations of the existing aggregates.

Diffusion NMR of model compounds

Figure 4 compares the hydrodynamic diameters estimated from experimentally acquired diffusion coefficients of the PAHs to hydrodynamic diameters predicted from Equation 4 for all seven model PAH compounds. As the SEGWE prediction yields the hydrodynamic diameters of single molecules and is based on molecular weight, any differences in diffusivity and, implicitly, hydrodynamic size can be attributed to the existence of nanoaggregates. Previous studies of natural asphaltenes suggests that formation of nanoaggregates in toluene is common, even at very low concentration (0.025% v/v).[39]

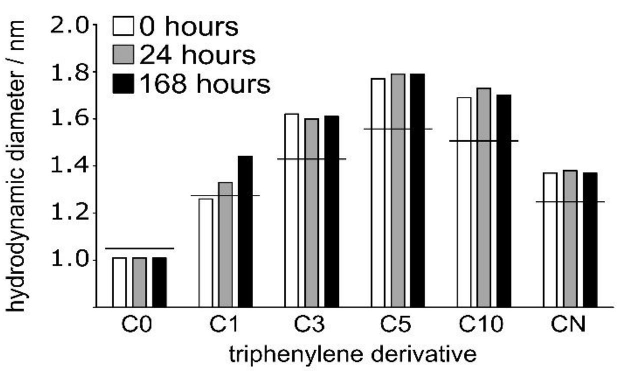

Figure 4. Experimentally acquired hydrodynamic diameters, acquired using diffusion NMR, for all seven model PAH compounds at 10 mg/mL in toluene-d_8, obtained at 0 (white bars), 24 (grey), and 168 hours (black) after sample preparation. Predicted hydrodynamic radii for single molecules in toluene-d_8 indicated by horizontal black bar.

Since both TPN-C0 and -C1 initially exhibit diffusion coefficients very similar to those predicted by Equation 4, it can be concluded that they present as single molecules immediately after mixing with toluene. However, DLS studies of TPN-C1 (Figure 3) reveal the presence of species with large hydrodynamic diameters. This discrepancy can be attributed to the complementarity of the two experimental methods. In DLS, large particles scatter more light than small ones, which prevents the smaller particles from being registered by the photodetector, while diffusion NMR methods are limited to hydrodynamic diameters of a few nanometers, i.e. individual molecules and nanoaggregates. Furthermore, the very low intensity of the sharp TPN-C1 peaks indicates that only a trace amount of the small species is present. The results of the combined techniques suggest that TPN-C1 forms large aggregates, well above the threshold for easy measurement by diffusion NMR, which are detected by DLS, while NMR captures remaining single TPN-C1 molecules immediately after addition to toluene. However, after 24 hours, stable nanoaggregates have formed, identified from the decrease in diffusion coefficient and corresponding increase in the estimated hydrodynamic diameter. Diffusion NMR data acquired for TPN-C3, -C5, and -C10 all reveal the presence of nanoaggregates in the solution, existing alongside the larger aggregates observed by DLS.

TPN-CN is captured in nanoaggregate form by NMR, coexisting with larger species that can only be observed by DLS. However, it was not possible to observe nanoaggregates for TPN-CNAcid. The ^{1}H NMR spectrum of TPN-CNAcid was very low in intensity, with broad signals in the aliphatic region indicating the presence of large aggregated species. With clear evidence of micrometre sized aggregates obtained using DLS methods, no diffusion NMR data from this species was included.

Molecular dynamics simulations: radial distribution functions

Radial distribution functions for four of the test set of model compounds, TPN-C0, C1, CN, and CNAcid, are presented in Figure 5. This subset of the PAHs has been chosen for direct comparison, as they have similar molecular weights (ca. 400 g mol^{-1}) but differ markedly in their chemical structures.

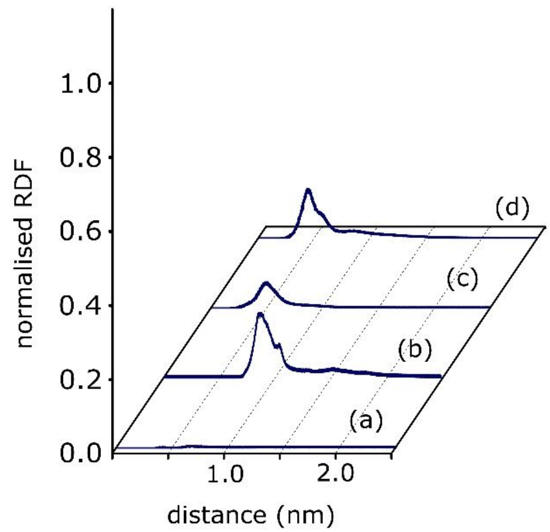

Figure 5. Normalised radial distribution functions of 7 molecules of (a) TPN-C0, (b) TPN-C1, (c) TPN-CN and (d) TPN-CNAcid, solvated by 700 toluene molecules, over a 100 ns simulation time.

No peak was observed in the RDF of TPN-C0, suggesting that there are no strong intermolecular interactions between TPN-C0 molecules, which agrees with both DLS and NMR results that individual molecules are solvated in toluene. The broad peak found in the RDF of TPN-C1 indicates the existence of aggregation over a large range of distances (from 0.7 nm to 1.1 nm). Its broad width, much greater than the characteristic distance for a parallel configuration (0.35 nm),[66] suggests that the aggregates formed could possess multiple configurations and could be in contact with each other at angles between 0° and 90°, forming non-parallel stacking configurations. This is consistent with the large hydrodynamic diameters observed by the DLS. The RDF plot of TPN-CN shows a broad peak between 0.3 nm and 0.7 nm, with a slow decay in intensity from 0.7 nm to 1.2 nm, which implies that aggregates are formed with various configurations, similar to that observed for TPN-C1. It is worth noting that the position of the main peak in the RDF indicates that energetically favourable parallel configurations are now preferred.[11] The TPN-CNAcid model compound also exhibits a major peak between 0.3 nm and 0.7 nm. For this PAH, there is also a distinct shoulder between 0.7 nm to 1.6 nm, implying the existence of loosely aggregated species.

The effect of the alkoxy chain length on aggregation can be observed by comparing RDFs for TPN-C1, C3, C5, and C10 (Figure 6). Data for TPN-C1 is include here to for comparison purpose.

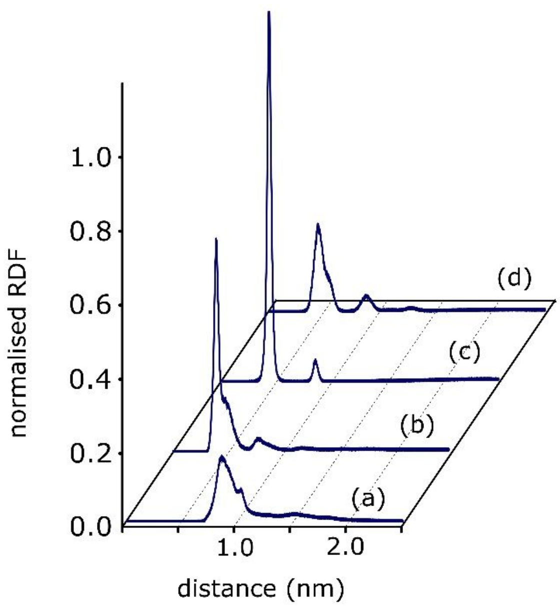

Figure 6. Normalised radial distribution functions of 7 molecules of (a) TPN-C1, (b) TPN-C3, (c) TPN-C5 and (d) TPN-C10, solvated by 700 toluene molecules, over a 100 ns simulation time.

DLS data shows that both TPN-C3 and -C5 form large aggregates instantly after being introduced into toluene, but then dissociated to 1 nm sized nanoaggregates after 24 hours and stayed stable afterwards. NMR measurements are in agreement, with these two model compounds forming nanoaggregates in a similar manner to natural asphaltenes.[1] The MD simulations presented here agree with both aspects of the experimental study. The narrow, well-defined peaks between 0.3 and 0.5 nm in the RDF, observed in both Figures 6b and 6c, suggest that both model compounds have a high potential for π-stacking. Additional peaks found at *ca*. 0.8 nm further support the existence of extended π-stacked aggregates of these model compounds.

TPN-C10 was found to be well solvated in toluene, with a hydrodynamic diameter around 1 nm reported by both DLS and NMR measurement (Figures 3 and 4). The broad RDF peak between 0.3 and 0.6 nm in Figure 6d, confirms that π-stacking is the main driving mechanism for nanoaggregate formation, with possible molecular configurations consistent with parallel π-stacking at 0.35 nm[66,67]. The RDF of TPN-C10 differs from -C3 and -C5 in two important ways. First, the distribution is broader. Second, the peak of the distribution for TPN-C10 indicates slightly larger distances between molecules. Both may be a result of the non-centrosymmetric structure of TPN-C10.

Molecular dynamics simulations of model compounds: distances between centers of mass

Distance between one of the seven PAH molecules and the other six in a given simulation box is plotted as a function of simulation time, providing an overview of the dynamic process of aggregation. Figure 7 shows the molecular distances for four model compounds: (a) TPN-C0, (b)TPN-C1, (c)TPN-CN, and (d)TPN-CNAcid. Each color corresponds to one of the six pairs of the PAH molecules. Various patterns can be seen here: random and scattered points suggest that Horizontal lines in these figures indicate the formation of aggregates with a characteristic distance. Formation of aggregates driven by π-stacking interaction will show a characteristic distance of 0.3-0.5 nm.[66,67] In the cases of large aggregates where more than two molecules are involved (dimers, trimers, tetramers), multiple horizontal lines will be observed in the figure. The number of parallel horizontal lines in the same figure indicate how many molecules have aggregated together.

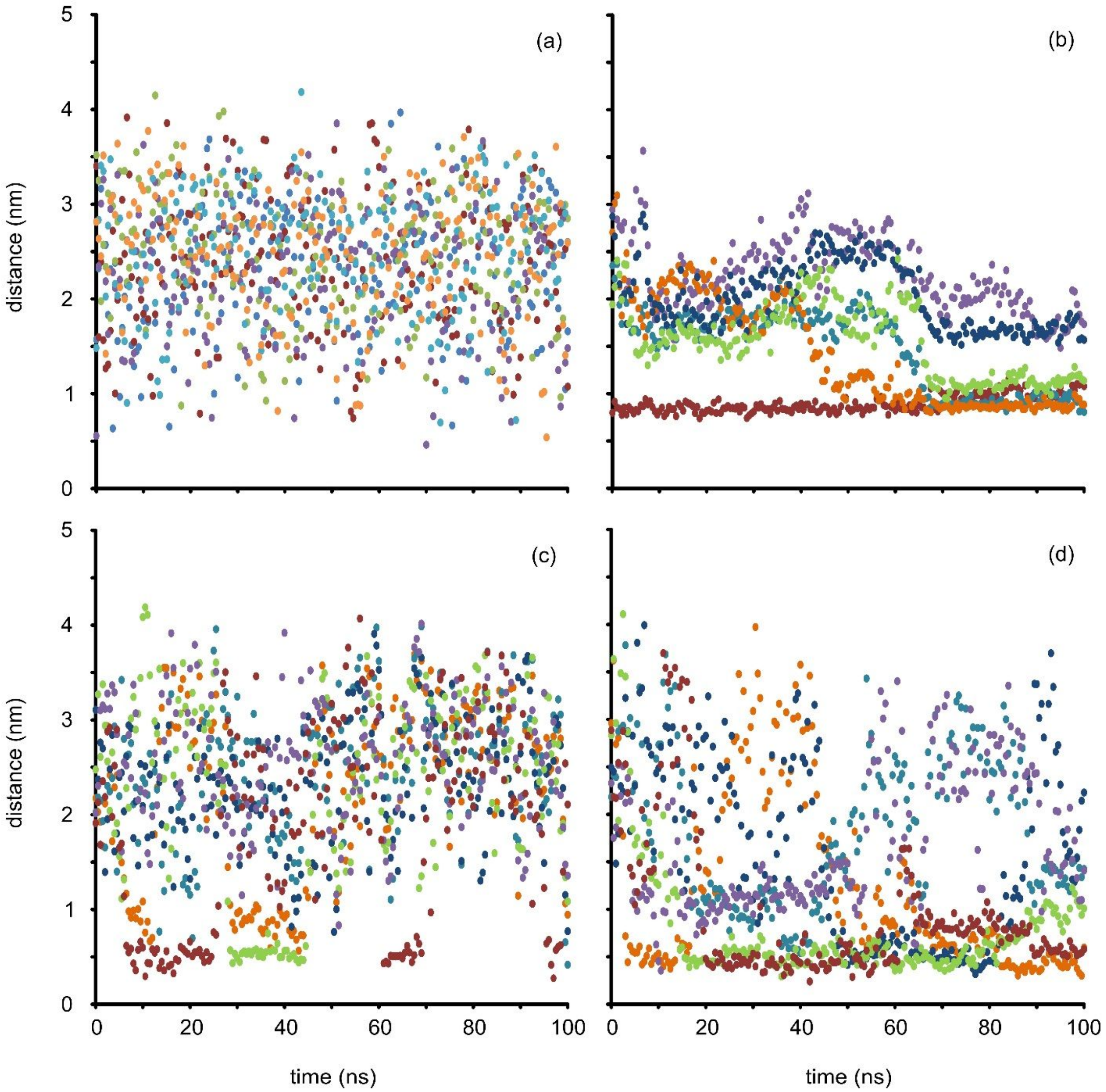

Figure 7. Calculated distances between the centers of mass (COM) for one molecule of model molecules of (a) TPN-C0, (b) TPN-C1, (c) TPN-CN, and (d) TPN-CNAcid, with the other 6 molecules present, during the 100 ns molecular dynamics simulation in toluene. Each color corresponds to one of the six pairs of the PAH molecules.

Only random distances between TPN-C0 molecules were observed during the 100 ns simulation time (Figure 7a) indicating no aggregation. This is fully consistent with both DLS and NMR results, as well as Figure 5a. As with Figure 5, the other three species presented here are all similar in molecular mass and all exhibited similar aggregation behaviour as revealed by both DLS and diffusion NMR. However, they differ in chemical structure, with key differences in the functional groups presents, and MD simulations suggest that the structures and dynamics of the aggregations formed are fundamentally different. Small distances (0.7-1.7 nm) between multiple pairs of TPN-C1 molecules, stable over longer periods of simulation time, can be observed in Figure 7b, indicating the formation of large aggregates and virtually no free molecules present in the sample. This is in agreement with the DLS measurements, where large TPN-C1 aggregates were observed, and also the NMR experiments, where only a small concentration of nanoaggregate PAH could be observed.

Figure 7c shows the formation of several TPN-CN dimers for short periods of time. Larger species can also be observed, such as a loosely associated trimer which forms at 30 ns and subsequently dissociates at 45 ns. The DLS data showed changes in the observed hydrodynamic diameter at both 24 and 168 hours, consistent with the simulation indicating that the molecule aggregates as a series of loosely formed configurations. TPN-CNAcid (Figure 7d) exhibits an increased number of associations compared with the amide, with a dimer forming immediately, a trimer at 15 ns, and a tetramer at 20 ns. The varying distances between pairs of TPN-CNAcid molecules suggest a constant assembling/disassembling process with multiple configurations, including parallel and non-parallel stacking, as well dissociation, as shown in the series of snapshots of the simulation below (Figure 8).

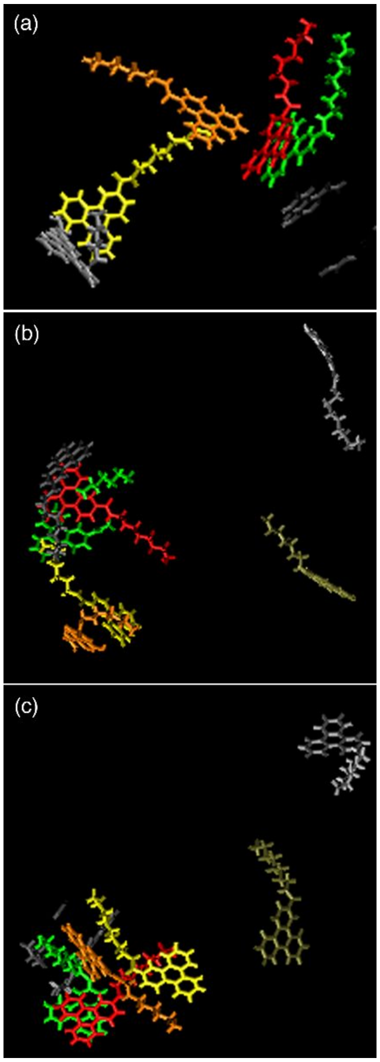

Figure 8. Snapshot of MD simulations of six molecules of TPN-CNAcid in toluene. Three possible configurations: (a) parallel stacking, (b) dissociation, and (c) non-parallel stacking, are observed in this set of images.

MD simulations also give insight into the role of alkoxy groups in PAH aggregation. Figures 9(a) to (d) show the distances between one molecule of model compounds ((a) TPN-C1 (repeated for context), (b)TPN-C3, (c)TPN-C5, and (d)TPN-C10) and six other model compound molecules in the same simulation box as a function of simulation time.

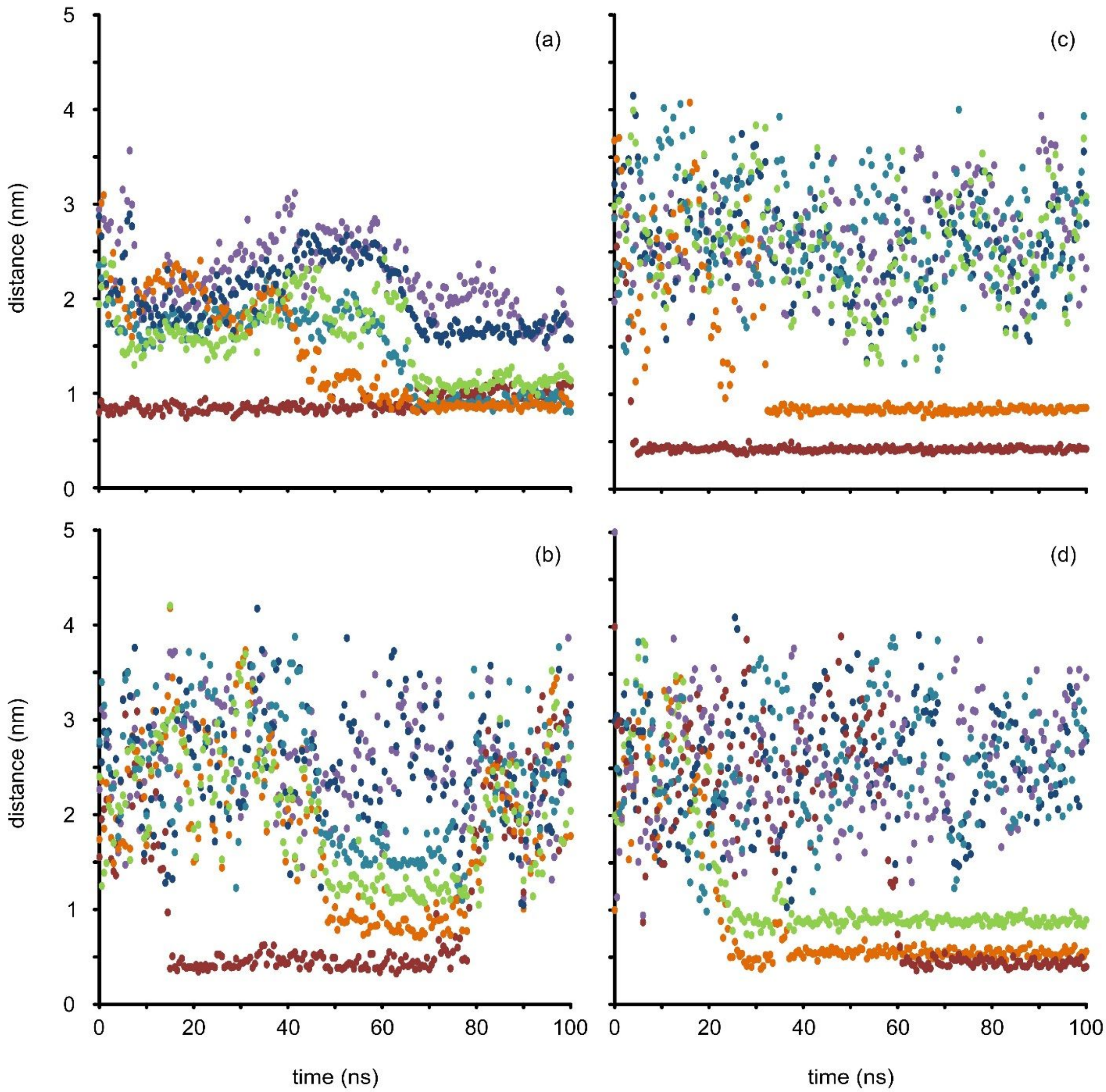

Figure 9. Calculated distances between the centers of mass (COM) for one molecule of model molecules of (a) TPN-C1 (repeated for context), (b) TPN-C3, (c) TPN-C5, and (d) TPN-C10, with the other 6 molecules present, during the 100 ns molecular dynamics simulation in toluene. Each color corresponds to one of the six pairs of the PAH molecules.

Figures 3 and 4 have already indicated key differences in the aggregates formed by TPNs -C1, -C3, -C5, and -C10. TPN-C1 forms large aggregates, with few molecules remaining un-aggregated in the sample. The other PAHs studied in this subset of the molecules, however, eventually form smaller nanoaggregate species. This behaviour is reproduced in Figure 9. In all three model compounds, TPN-C3, -C5, and -C10, the horizontal lines indicate the formation of stable aggregates between limited numbers of PAH molecules, while the remaining points in the Figures indicate very few interactions between the aggregates and the remaining molecules in the simulation box. TPN-C3 forms well-defined aggregates with distances between the PAHs consistent with π-stacking of pairs and triplets of molecules. Both DLS and NMR indicate the presence of nanometer sized species in the sample. TPN-C5 forms more loosely aggregated species with a number of molecules forming at distances consistent with a parallel, π-stacked, aggregate. TPN-C10 forms dimers, trimers and even a tetramer can be observed at 60 ns (Figure 9d). For both PAHs, the aggregate size is still in the range of 1 to 2 nanometers, again consistent with both DLS and NMR studies.

Figures 7 and 9 together suggest that there are three possible arrangement between PAHs molecules in toluene: dissociation (large intermolecular distance, no horizontal lines in the figures); aggregation with random configuration (intermediate intermolecular distance); and aggregation with parallel configuration (short intermolecular distance, close to *ca*. 0.35 nm).

DISCUSSION

Effect of acid and amide groups on aggregation

Light scattering results of TPN-CN and TPN-CNAcid (Figure 3), containing amide and carboxylic acid groups respectively, indicate that both compounds form large aggregates instantly in toluene. The measured sizes of the aggregates was not constant, implying that these model compounds could aggregate into large and unstable clusters for an extended period of time. Broad peaks (0.3 to 1.3 nm) observed in RDF plots of TPN-CN and TPN-CNAcid suggest that the aggregates formed have multiple configurations with a low packing density. According to RDF and gdist data (Figure 7b), it is possible that TPN-CN and -CNAcid can form stable nanoaggregates with parallel configuration, which could subsequently form loose clusters as observed by DLS measurements.

Previous density functional theory studies concluded that parallel configurations are the most energetically favourable state for natural asphaltenes, with a characteristic intermolecular distance of ca. 0.35 nm,.[69-75] It is likely that the large aggregates formed would continuously re-assemble into more stable configurations, driven by the weaker van der Waals forces between the aromatic cores.[14,15] Addition of polar groups, such as carboxylic acids and amides, increases the polarity of the model PAHs, which consequently enhances the potential for aggregation. Instead of the well-defined peaks that are characteristics of π-stacking, the molecular dynamics simulations here show broader peaks radial distribution functions with a number of association-dissociation events on a nanosecond timescale. It is very likely that introducing polar groups into PAHs not only improves the possibility for aggregation, but also expands the range of molecular configurations available within the PAH aggregates. The synergistic effect of them results in an increased size of aggregates formed, as demonstrated by the large aggregates measured by DLS and previous studies[23].

Effect of alkoxy chain length on aggregation

Previous studies of molecules possessing similar chemical structures suggest that the alkyl chains surrounding the triphenylene core have the following two roles: stabilization of the formed discotic liquid crystal columns and control of the distance between the columns.[28] Our experimental results show that TPN-C1 forms large aggregates (above 1000 nm) over a prolonged period of time. One of the possible causes of such aggregation is crystallization of the PAHs, resulting in large particles of micrometer size. However, it is more likely that, upon such strong attractive interaction, TPN-C1 molecules could aggregate in various configurations - the methyl side chains are too short to limit with parallel configurations solely. The increased number of configurations available facilitates the formation of aggregates with potentially random configurations and a wide range of size distribution. Once the large aggregates formed precipitate and sediment, there are only small aggregated dispersed in the suspension. This is supported by the diffusion NMR results - single molecules rather than large aggregates were detected for TPN-C1, which is also supported by simulation results that the RDF of TPN-C1 is also notably broader than both TPN-C3 and –C5.

Once the side chains are of sufficient length, as found in TPN-C3, -C5, and -C10, they can effectively counter the aggregation potential and enhance the stability of the nanoaggregates formed. This is consistent with literature where aliphatic side chains were reported to improve the stability of asphaltene nanoaggregates.[80] The configurational constraints imposed by the aliphatic side-chains increase proportionally to their length (TPN-C1 to TPN-C3 to TPN-C5), because parallel configurations become increasingly energetically favourable. The limited size of the aggregates can be mainly attributed to the aromatic nature of the solvent,[81,82] and the length of the side-chains enforcing a parallel configuration.[12]

TPN-C10 differs from the other three alkoxy-substituted triphenylenes in that it has an additional, single C_{10} chain that renders the molecule asymmetric. Both experimental methods record only nanometer-sized aggregates forming, while the MD simulations indicate a broader RDF and aggregations at distances larger than the characteristic π-stacking distance. This suggests that the decyl chain in TPN-C10 inhibits the aggregation of the PAH, perhaps enabling the solvent to penetrate the single columns easily and breaking up interactions between the PAH molecules.

Increasingly longer side-chains are known to hinder/limit aggregation in natural asphaltenes,[12] which might explain the difference in the stabilisation time between the model compounds. Investigations of asymmetric compounds suggest that long chains hinder the aggregation of PAHs and limit the size to which the nanoaggregates could form.[83,84] Other studies further support this mechanism by removing long side chains from model compounds, which allows the molecules to achieve a more energetically favourable state as better ordered/more densely packed nanoaggregates.[85] The behaviour of TPN-C10 in our study reflects these previous observations.

CONCLUSIONS

Seven model compounds based on triphenylene were synthesized and evaluated by measuring their hydrodynamic diameters over a 168 hour period, using both light scattering and diffusion NMR methodologies. The experimental results were further supported by MD simulations. We show that complementary experimental methods should be deployed when examining such colloidal systems, e.g. asphaltene suspended in toluene, as the aggregates formed can span multiple length scales.

The series of model compounds developed in this study reveal how subtle changes in chemical structure, such as small increases in alkyl chain lengths, can significantly impact the aggregation of the compounds. An increased chain length surrounding the triphenylene core (e.g. TPN-C3 and -C5) can facilitate ordered configurations (such as π-stacking) upon the nanoaggregates, but introducing asymmetry to the molecular architecture (e.g. TPN-C10) enhances solvation potential. The addition of functional groups (e.g. TPN-CN and -CNAcid) leads to the formation of large aggregates that are loosely packed and constantly re-configuring. The observation demonstrates that the attraction between aromatic cores can be countered by the degree of solvation by toluene as well steric hindrance imposed by the side chains.

These results confirm that the aggregation of PAHs is determined by the fine balance between 1) π-π interactions between the aromatic cores; 2) interactions between polar groups; 3) steric hindrance caused by the side chains, and 4) the degree of solvation by toluene. The structure and size of the final aggregated species is determined by the balance between these different driving forces. Polyaromatic hydrocarbons commonly present a wide range of side-chains of different lengths, which vary the nanoaggregate interactions. However, there are clear effects that these different chain lengths and functional groups have on their aggregation pathways. In turn, better understanding of the effects of specific functional groups on the aggregation will help to develop strategies to counter this clustering and improve the use of PAHs, such as natural asphaltenes, in applied and industrial chemical settings.

Supporting Information.

AUTHOR INFORMATION

Corresponding Author

*Zhenyu J. Zhang: Z.J.Zhang@bham.ac.uk; Rob Evans: r.evans2@aston.ac.uk

Present Addresses

Raphael Laurent present address: Department of Materials, École Polytechnique Universitaire de Montpellier, Montpellier, 34095 France

Author Contributions

The manuscript was written through contributions of all authors. All authors have given approval to the final version of the manuscript.

Acknowledgment

ZJZ thanks EPSRC (grant EP/P007864/1) for financial support. The diffusion NMR experiments were funded by the RSC Research Fund RF17-3528. RL would like to thank ERASMUS for the opportunity to study in England, and for support throughout.

Supporting Information

- Synthesis of Model Polyaromatic Hydrocarbons
- Diffusion NMR
- Additional images of Molecular Dynamics simulations

REFERENCES

1. Mullins, O. C., The Modified Yen Model. *Energy Fuels* **2010**, *24* (4), 2179-2207.
2. Sabbah, H.; Morrow, A. L.; Pomerantz, A. E.; Zare, R. N., Evidence for Island Structures as the Dominant Architecture of Asphaltenes. *Energy Fuels* **2011**, *25* (4), 1597-1604.
3. Groenzin, H.; Mullins, O. C., Asphaltene Molecular Size and Structure. *J. Phys. Chem. A* **1999**, *103* (50), 11237-11245.
4. Mullins, O. C.; Sabbah, H.; Eyssautier, J.; Pomerantz, A. E.; Barré, L.; Andrews, A. B.; Ruiz-Morales, Y.; Mostowfi, F.; McFarlane, R.; Goual, L., Advances in Asphaltene Science and the Yen–Mullins Model. *Energy Fuels* **2012**, *26* (7), 3986-4003.
5. Alshareef, A. H.; Scherer, A.; Tan, X.; Azyat, K.; Stryker, J. M.; Tykwinski, R. R.; Gray, M. R., Formation of Archipelago Structures during Thermal Cracking Implicates a Chemical Mechanism for the Formation of Petroleum Asphaltenes. *Energy Fuels* **2011**, *25* (5), 2130-2136.
6. Kuznicki, T.; Masliyah, J. H.; Bhattacharjee, S., Molecular Dynamics Study of Model Molecules Resembling Asphaltene-Like Structures in Aqueous Organic Solvent Systems. *Energy Fuels* **2008**, *22* (4), 2379-2389
7. Hammami, A.; Ratulowski, J., Precipitation and Deposition of Asphaltenes in Production Systems: A Flow Assurance Overview. In *Asphaltenes, heavy oils, and petroleomics*, Springer: New York, NY, **2007**; pp 617-660.
8. Haji-Akbari, N.; Masirisuk, P.; Hoepfner, M. P.; Fogler, H. S., A Unified Model for Aggregation of Asphaltenes. *Energy Fuels* **2013**, *27* (5), 2497-2505
9. Murgich, J., Intermolecular Forces in Aggregates of Asphaltenes and Resins. *Petrol. Sci. Technol.* **2002**, *20* (9-10), 983-997.
10. Adams, J. J., Asphaltene Adsorption, a Literature Review. *Energy Fuels* **2014**, *28* (5), 2831-2856.
11. Tan, X.; Fenniri, H.; Gray, M. R., Pyrene Derivatives of 2,2′-Bipyridine as Models for Asphaltenes: Synthesis,

Characterization, and Supramolecular Organization. *Energy Fuels* **2007**, *22* (2), 715-720.
12. Jian, C.; Tang, T.; Bhattacharjee, S., Probing the Effect of Side-Chain Length on the Aggregation of a Model Asphaltene Using Molecular Dynamics Simulations. *Energy Fuels* **2013**, *27* (4), 2057-2067.
13. Kuznicki, T.; Masliyah, J. H.; Bhattacharjee, S., Aggregation and Partitioning of Model Asphaltenes at Toluene−Water Interfaces: Molecular Dynamics Simulations. *Energy Fuels* **2009**, *23* (10), 5027-5035.
14. Nordgård, E. L.; Sørland, G.; Sjöblom, J., Behavior of Asphaltene Model Compounds at W/O Interfaces. *Langmuir* **2009**, *26* (4), 2352-2360.
15. Nordgård, E. L. k.; Sjöblom, J., Model Compounds for Asphaltenes and C_{80} Isoprenoid Tetraacids. Part I: Synthesis and Interfacial Activities. *J. Dispersion Sci. Technol.* **2008**, *29* (8), 1114-1122.
16. Burya, Y. G.; Yudin, I. K.; Dechabo, V. A.; Kosov, V. I.; Anisimov, M. A., Light-scattering Study of Petroleum Asphaltene Aggregation. *Appl. Opt.* **2001**, *40* (24), 4028-4035.
17. Yudin, I.; Nikolaenko, G.; Gorodetskii, E.; Markhashov, E.; Agayan, V.; Anisimov, M.; Sengers, J., Crossover Kinetics of Asphaltene Aggregation in Hydrocarbon Solutions. *Phys. A* 1998, *251* (1), 235-244.
18. Pisula, W.; Tomović, Ž.; Simpson, C.; Kastler, M.; Pakula, T.; Müllen, K., Relationship between Core Size, Side Chain Length, and the Supramolecular Organization of Polycyclic Aromatic Hydrocarbons. *Chem. Mater.* **2005**, *17* (17), 4296-4303.
19. Akbarzadeh, K.; Bressler, D. C.; Wang, J.; Gawrys, K. L.; Gray, M. R.; Kilpatrick, P. K.; Yarranton, H. W., Association Behavior of Pyrene Compounds as Models for Asphaltenes. *Energy Fuels* **2005**, *19* (4), 1268-1271.
20. Mullins, O. C., Review of the Molecular Structure and Aggregation of Asphaltenes and Petroleomics. *SPE J.* **2008**, *13* (01), 48-57.
21. Stachowiak, C.; Viguié, J.-R.; Grolier, J.-P. E.; Rogalski, M., Effect of n-Alkanes on Asphaltene Structuring in Petroleum Oils. *Langmuir* **2005**, *21* (11), 4824-4829.
22. Breure, B.; Subramanian, D.; Leys, J.; Peters, C. J.; Anisimov, M. A., Modeling Asphaltene Aggregation with a Single Compound. *Energy Fuels* **2012**, *27* (1), 172-176.
23. Sjöblom, J.; Simon, S.; Xu, Z., Model Molecules Mimicking Asphaltenes. *Adv. Colloid Interface Sci.* **2015**, *218*, 1-16.
24. Lundblad, R. L., *Chemical reagents for protein modification*. CRC press, **2014**.
25. Chandrasekhar, S., Columnar, Discotic Nematic and Lamellar Liquid Crystals: Their Structures and Physical Properties. *Handbook*

of Liquid Crystals: Low Molecular Weight Liquid Crystals II **1998**, 749-780.
26. Kumar, S., Triphenylene-based Discotic Liquid Crystal Dimers, Oligomers and Polymers. *Liq. Cryst.* **2005**, *32* (9), 1089-1113.
27. Heeger, A. J., Semiconducting and Metallic Polymers: The Fourth Generation of Polymeric Materials (Nobel Lecture). *Angew. Chem. Int. Ed.* **2001**, *40* (14), 2591-2611.
28. Kumar, S., Recent Developments in the Chemistry of Triphenylene-based Discotic Liquid Crystals. *Liq. Cryst.* **2004**, *31* (8), 1037-1059.
29. Setoguchi, Y.; Monobe, H.; Wan, W.; Terasawa, N.; Kiyohara, K.; Nakamura, N.; Shimizu, Y., Infrared Studies on Hydrogen Bond Interaction in a Homologues |Series of Triphenylene Discotic Liquid Crystals having Carboxylic Acids at the Peripheral Chains. *Thin Solid Films* **2003**, *438*, 407-413.
30. Nalwaya, V.; Tantayakom, V.; Piumsomboon, P.; Fogler, S., Studies on Asphaltenes through Analysis of Polar Fractions. *Ind. Eng. Chem. Res.* **1999**, *38* (3), 964-972.
31. Kaminski, T. J.; Fogler, H. S.; Wolf, N.; Wattana, P.; Mairal, A., Classification of Asphaltenes via Fractionation and the Effect of Heteroatom Content on Dissolution Kinetics. *Energy Fuels* **2000**, *14* (1), 25-30.
32. Fish, R. H.; Komlenic, J. J.; Wines, B. K., Characterization and Comparison of Vanadyl and Nickel Compounds in Heavy Crude Petroleums and Asphaltenes by Reverse-Phase and Size-Exclusion Liquid Chromatography/Graphite Furnace Atomic Absorption Spectrometry. *Anal. Chem.* **1984**, *56* (13), 2452-2460.
33. Ancheyta, J.; Centeno, G.; Trejo, F.; Marroquin, G.; Garcia, J.; Tenorio, E.; Torres, A., Extraction and Characterization of Asphaltenes from Different Crude Oils and Solvents. *Energy Fuels* **2002**, *16* (5), 1121-1127.
34. Agrawala, M.; Yarranton, H. W., An Asphaltene Association Model Analogous to Linear Polymerization. *Ind. Eng. Chem. Res.* **2001**, *40* (21), 4664-4672.
35. Strausz, O. P.; Mojelsky, T. W.; Lown, E. M., The Molecular Structure of Asphaltene: An Unfolding Story. *Fuel* **1992**, *71* (12), 1355-1363.
36. Teklebrhan, R. B.; Ge, L.; Bhattacharjee, S.; Xu, Z.; Sjöblom, J., Probing Structure–Nanoaggregation Relations of Polyaromatic Surfactants: A Molecular Dynamics Simulation and Dynamic Light Scattering Study. *J. Phys. Chem. B.* **2012**, *116* (20), 5907-5918.
37. Eyssautier, J. l.; Frot, D.; Barré, L., Structure and Dynamic Properties of Colloidal Asphaltene Aggregates. *Langmuir* **2012**, *28* (33), 11997-12004.
38. Hemmati-Sarapardeh, A.; Dabir, B.; Ahmadi, M.; Mohammadi, A. H.; Husein, M. M., Toward Mechanistic Understanding of Asphaltene

Aggregation Behavior in Toluene: The Roles of Asphaltene Structure, Aging Time, Temperature, and Ultrasonic Radiation. *J. Mol. Liq.* **2018**, *264*, 410-424.
39. Mansur, C. R. E.; de Melo, A. R.; Lucas, E. F., Determination of Asphaltene Particle Size: Influence of Flocculant, Additive, and Temperature. *Energy Fuels* **2012**, *26* (8), 4988-4994.
40. Johnson, C. S., Diffusion-Ordered Nuclear Magnetic Resonance Spectroscopy: Principles and Applications. *Prog. Nucl. Magn. Reson. Spectrosc.* **1999**, *34* (3-4), 203-256.
41. Stejskal, E. O.; Tanner, J. E., Spin Diffusion Measurements: Spin Echoes in the Presence of a Time-Dependent Field Gradient. *J. Chem. Phys.* **1965**, *42* (1), 288-292.
42. Durand, E.; Clemancey, M.; Lancelin, J.-M.; Verstraete, J.; Espinat, D.; Quoineaud, A.-A., Aggregation States of Asphaltenes - Evidence of Two Chemical Behaviours by ^{1}H Diffusion-Ordered Nuclear Magnetic Resonance Spectroscopy. *J. Phys. Chem. C* **2009**, *113* (36), 16266 - 16276.
43. Jones, M.; Taylor, S. E., NMR Relaxometry and Diffusometry in Characterizing Structural, Interfacial and Colloidal Properties of Heavy Oils and Oil Sands. *Adv. Colloid Interface Sci.* **2015**, *224*, 33-45.
44. Durand, E.; Clemancey, M.; Quoineaud, A.-A.; Verstraete, J.; Espinat, D.; Lancelin, J.-M., ^{1}H Diffusion-Ordered Spectroscopy (DOSY) Nuclear Magnetic Resonance (NMR) as a Powerful Tool for the Analysis of Hydrocarbon Mixtures and Asphaltenes. *Energy Fuels* **2008**, *22* (4), 2604-2610.
45. Durand, E.; Clemancey, M.; Lancelin, J.-M.; Verstraete, J.; Espinat, D.; Quoineaud, A.-A., Effect of Chemical Composition on Asphaltenes Aggregation. *Energy Fuels* **2010**, *24* (2), 1051-1062.
46. Östlund, J.-A.; Wattana, P.; Nydén, M.; Fogler, H. S., Characterization of Fractionated Asphaltenes by UV−vis and NMR Self-Diffusion Spectroscopy. *J. Colloid Interface Sci.* **2004**, *271* (2), 372-380.
47. Norinaga, K.; Wargardalam, V. J.; Takasugi, S.; Iino, M.; Matsukawa, S., Measurement of Self-Diffusion Coefficient of Asphaltene in Pyridine by Pulsed Field Gradient Spin−Echo ^{1}H NMR. *Energy Fuels* **2001**, *15* (5), 1317-1318.
48. Kawashima, H.; Takanohashi, T.; Iino, M.; Matsukawa, S., Determining Asphaltene Aggregation in Solution from Diffusion Coefficients As Determined by Pulsed Field Gradient Spin Echo ^{1}H NMR. *Energy Fuels* **2008**, *22*, 3989-3993.
49. Gao, F.; Xu, Z.; Liu, G.; Yuan, S., Molecular Dynamics Simulation: The Behavior of Asphaltene in Crude Oil and at the Oil/Water Interface. *Energy Fuels* **2014**, *28* (12), 7368-7376.
50. Korb, J.-P.; Louis-Joseph, A.; Benamsili, L. s., Probing Structure and Dynamics of Bulk and Confined Crude Oils by

Multiscale NMR Spectroscopy, Diffusometry, and Relaxometry. *J. Phys. Chem. B.* **2013**, *117* (23), 7002-7014.
51. Tanga, M.; Davis, R.; Reist, E., Synthesis of phenanthro [9, 10-g] isoquinoline. *J. Heterocycl. Chem.* **1987**, *24* (1), 39-41.
52. Pecora, R., *Dynamic light scattering: applications of photon correlation spectroscopy*. Springer, New York, NY, USA, 2013.
53. Vaccaro, A.; Šefčík, J.; Morbidelli, M., Characterization of colloidal polymer particles through stability ratio measurements. *Polymer* **2005**, *46* (4), 1157-1167.
54. Nilsson, M., The DOSY Toolbox: A New Tool for Processing PFG NMR Diffusion Data. *J. Magn. Reson.* **2009**, *200* (2), 296-302.
55. Jerschow A.; MullerN., Suppression of Convection Artifacts in Stimulated-Echo Diffusion Experiments. Double-Stimulated-Echo Experiments. *J. Magn. Reson.*, **1997**, *125*, 372–375.
56. Einstein, A., The Motion of Elements Suspended in Static Liquids as Claimed in the Molecular Kinetic Theory of Heat. *Ann. Phys.* **1905**, *17* (8), 549-560.
57. Gierer, A.; Wirtz, K., Molekulare Theorie der Mikroreibung. *Z. Naturforsch.* **1953**, *8* (9), 532-538.
58. Evans, R.; Deng, Z.; Rogerson, A. K.; McLachlan, A. S.; Richards, J. J.; Nilsson, M.; Morris, G. A., Quantitative Interpretation of Diffusion-Ordered NMR Spectra: Can We Rationalize Small Molecule Diffusion Coefficients? *Angew. Chem., Int. Ed.* **2013**, *52* (11), 3199-3202.
59. Evans, R.; Dal Poggetto, G.; Nilsson, M.; Morris, G. A., Improving the Interpretation of Small Molecule Diffusion Coefficients. *Anal. Chem.* **2018**, *90* (6), 3987-3994.
60. Jian, C. Molecular Dynamics Investigation on the Aggregation of Polyaromatic Compounds in Water and Organic Solvents. University of Alberta, Alberta, Canada, 2015.
61. van der Spoel, D., Lindahl, E., Hess, B. and The Gromacs Development Team, *Gromacs User Manual Version 4.6.5*. **2013**.
62. Jorgensen, W. L.; Maxwell, D. S.; Tirado-Rives, J., Development and Testing of the OPLS All-Atom Force Field on Conformational Energetics and Properties of Organic Liquids. *J. Am. Chem. Soc.* **1996**, *118* (45), 11225-11236..
63. Boek, E. S.; Yakovlev, D. S.; Headen, T. F., Quantitative Molecular Representation of Asphaltenes and Molecular Dynamics Simulation of Their Aggregation. *Energy Fuels* **2009**, *23* (3), 1209-1219.
64. Headen, T. F.; Boek, E. S.; Skipper, N. T., Evidence for Asphaltene Nanoaggregation in Toluene and Heptane from Molecular Dynamics Simulations. *Energy Fuels* **2009**, *23* (3), 1220-1229.
65. Costa, J.; Simionesie, D.; Mulheran, P.; Zhang, Z., Aggregation of Model Asphaltenes: A Molecular Dynamics Study. *J. Phys. Condens. Matter* **2016**, *28* (39), 394002.

66. Moreira da Costa, L.; Stoyanov, S. R.; Gusarov, S.; Seidl, P. R.; Walkimar de M. Carneiro, J.; Kovalenko, A., Computational Study of the Effect of Dispersion Interactions on the Thermochemistry of Aggregation of Fused Polycyclic Aromatic Hydrocarbons as Model Asphaltene Compounds in Solution. *J. Phys. Chem. A* **2014**, *118* (5), 896-908.
67. Schulze, B. M.; Watkins, D. L.; Zhang, J.; Ghiviriga, I.; Castellano, R. K., Estimating the Shape and Size of Supramolecular Assemblies by Variable Temperature Diffusion-Ordered Spectroscopy. *Org. Biomol. Chem.* **2014**, *12* (40), 7932-7936.
68. Alameddine, B.; Aebischer, O. F.; Amrein, W.; Donnio, B.; Deschenaux, R.; Guillon, D.; Savary, C.; Scanu, D.; Scheidegger, O.; Jenny, T. A., Mesomorphic Hexabenzocoronenes Bearing Perfluorinated Chains. *Chem. Mater.* **2005**, *17* (19), 4798-4807.
69. Groenzin, H.; Mullins, O. C., Molecular Size and Structure of Asphaltenes from Various Sources. *Energy Fuels* **2000**, *14* (3), 677-684.
70. Groenzin, H.; Mullins, O. C., Asphaltene Molecular Size and Weight by Time-Resolved Fluorescence Depolarization. *Asphaltenes, heavy oils, and petroleomics* Springer, New York, NY, USA, **2007**.
71. Alvarez-Ramirez, F.; Ramirez-Jaramillo, E.; Ruiz-Morales, Y., Calculation of the Interaction Potential Curve between Asphaltene−Asphaltene, Asphaltene−Resin, and Resin−Resin Systems Using Density Functional Theory. *Energy Fuels* **2006**, *20* (1), 195-204.
72. Harris, J., Simplified Method for Calculating the Energy of Weakly Interacting Fragments. *Phys. Rev. B* **1985**, *31* (4), 1770.
73. Vosko, S. H.; Wilk, L.; Nusair, M., Accurate Spin-Dependent Electron Liquid Correlation Energies for Local Spin Density Calculations: A Critical Analysis. *Can. J. Phys.* **1980**, *58* (8), 1200-1211.
74. Perdew, J. P.; Wang, Y., Accurate and Simple Analytic Representation of the Electron-Gas Correlation Energy. *Phys. Rev. B* **1992**, *45* (23), 13244.
75. Delley, B., An All-Electron Numerical Method for Solving the Local Density Functional for Polyatomic Molecules. *J. Chem. Phys.* **1990**, *92* (1), 508-517.
76. Kumar, S., Triphenylene-based Discotic Liquid Crystal Dimers, Oligomers and Polymers. *Liq. Cryst.* **2005**, *32* (9), 1089-1113.
77. Bast, T.; Hentschke, R., Molecular Dynamics Simulation of a Micellar System: 2,3,6,7,10,11-Hexakis(1,4,7-trioxaoctyl)triphenylene in Water. *J. Phys. Chem.* **1996**, *100* (30), 12162-12171.
78. Sinnokrot, M. O.; Sherrill, C. D., High-Accuracy Quantum Mechanical Studies of π−π Interactions in Benzene Dimers. *J. Phys. Chem. A* **2006**, *110* (37), 10656-10668.

79. Martinez, C. R.; Iverson, B. L., Rethinking the Term “pi-stacking”. *Chem. Sci.* **2012**, *3* (7), 2191-2201.
80. Takanohashi, T.; Sato, S.; Saito, I.; Tanaka, R., Molecular Dynamics Simulation of the Heat-Induced Relaxation of Asphaltene Aggregates. *Energy Fuels* **2003**, *17* (1), 135-139.
81. Van der Hoeven, P. C.; Lyklema, J., Electrostatic Atabilization in Non-Aqueous Media. *Adv. Colloid Interface Sci.* **1992**, *42*, 205-277.
82. Wang, S.; Liu, J.; Zhang, L.; Masliyah, J.; Xu, Z., Interaction Forces between Asphaltene Surfaces in Organic Solvents. *Langmuir* **2009**, *26* (1), 183-190.
83. Andreatta, G.; Goncalves, C. C.; Buffin, G.; Bostrom, N.; Quintella, C. M.; Arteaga-Larios, F.; Pérez, E.; Mullins, O. C., Nanoaggregates and Structure-Function Relations in Asphaltenes. *Energy Fuels* **2005**, *19* (4), 1282-1289.
84. Zeng, H.; Song, Y.-Q.; Johnson, D. L.; Mullins, O. C., Critical Nanoaggregate Concentration of Asphaltenes by Direct-Current (DC) Electrical Conductivity. *Energy Fuels* **2009**, *23* (3), 1201-1208.
85. Trejo, F.; Ancheyta, J.; Rana, M. S., Structural Characterization of Asphaltenes Obtained from Hydroprocessed Crude Oils by SEM and TEM. *Energy Fuels* **2009**, *23* (1), 429-439.

Table of Contents Graphic

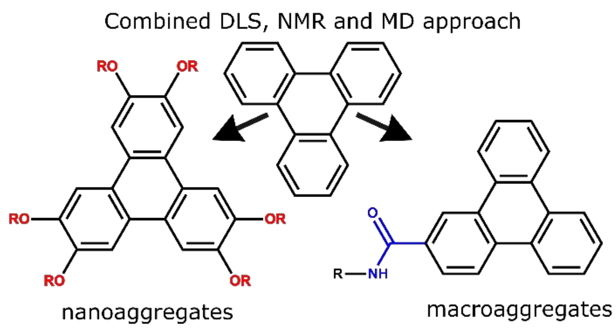

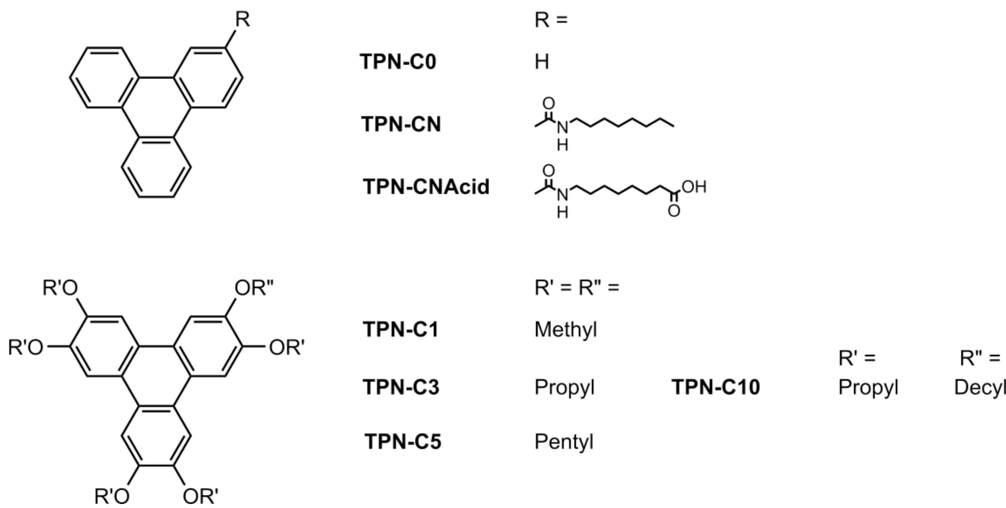

Figure 1. Chemical structures of the seven triphenylene derivatives used in the present study.

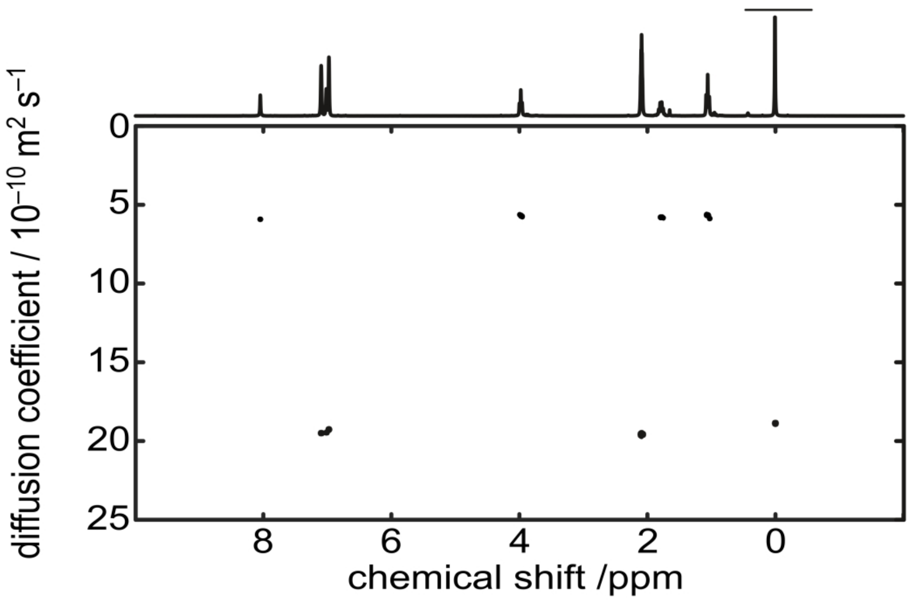

Figure 2. Representative DOSY spectrum of TPN-C3 in toluene-d_8. All experimental details of diffusion NMR study are included in the Supplementary Information.

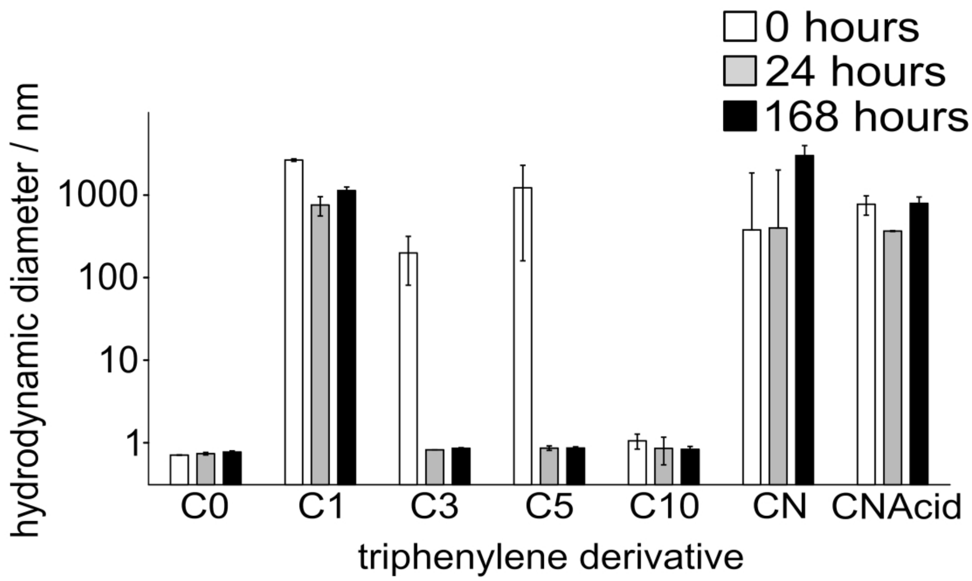

Figure 3. Averaged hydrodynamic diameters for all seven model PAH compounds at 10 mg/mL, acquired using dynamic light scattering at an angle of 173°, in toluene at 0 (white), 24 (grey), and 168 hours (black) after sample preparation.

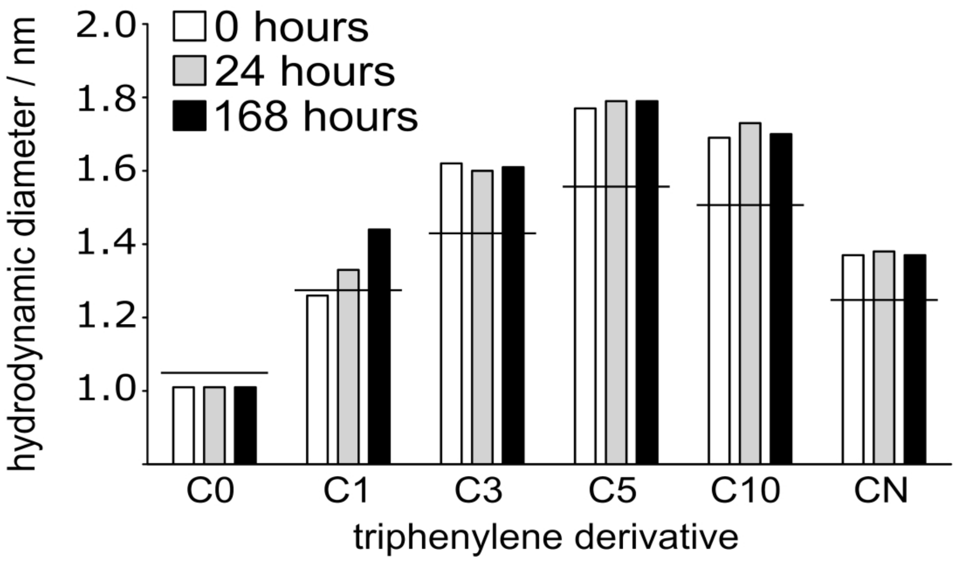

Figure 4. Experimentally acquired hydrodynamic diameters, acquired using diffusion NMR, for all seven model PAH compounds at 10 mg/mL in toluene-d_8, obtained at 0 (white bars), 24 (grey), and 168 hours (black) after sample preparation. Predicted hydrodynamic radii for single molecules in toluene-d8 indicated by horizontal black bar.

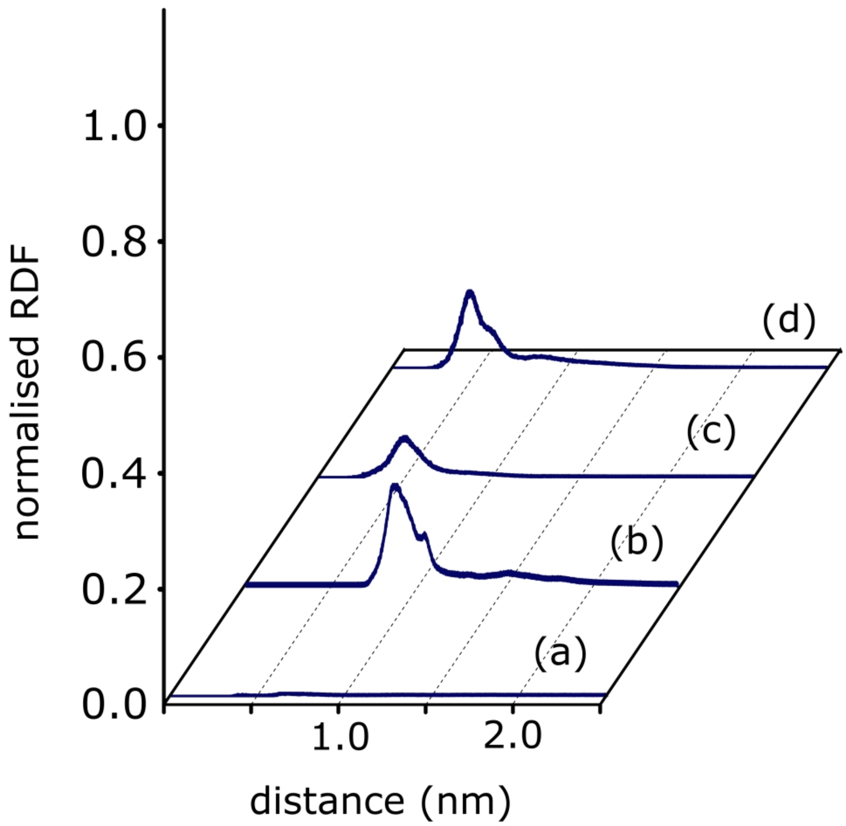

Figure 5. Normalised radial distribution functions of 7 molecules of (a) TPN-C0, (b) TPN-C1, (c) TPN-CN and (d) TPN-CNAcid, solvated by 700 toluene molecules, over a 100 ns simulation time.

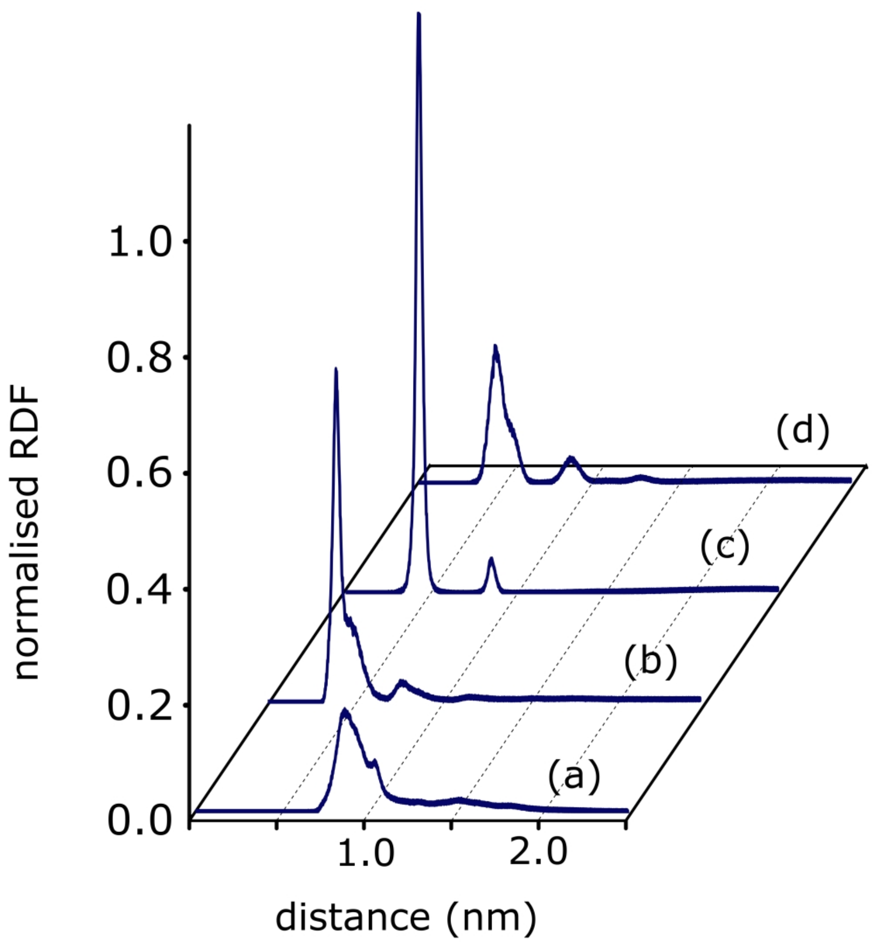

Figure 6. Normalised radial distribution functions of 7 molecules of (a) TPN-C1, (b) TPN-C3, (c) TPN-C5 and (d) TPN-C10, solvated by 700 toluene molecules, over a 100 ns simulation time.

Unable to Convert Image

The dimensions of this image (in pixels) are too large to be converted. For this image to convert, the total number of pixels (height x width) must be less than 40,000,000 (40 megapixels).

Figure 7. Calculated distances between the centers of mass for one molecule of model molecules of (a) TPN-C0, (b) TPN-C1, (c) TPN-CN, and (d) TPN-CNAcid, with the other 6 molecules present, during the 100 ns molecular dynamics simulation in toluene.

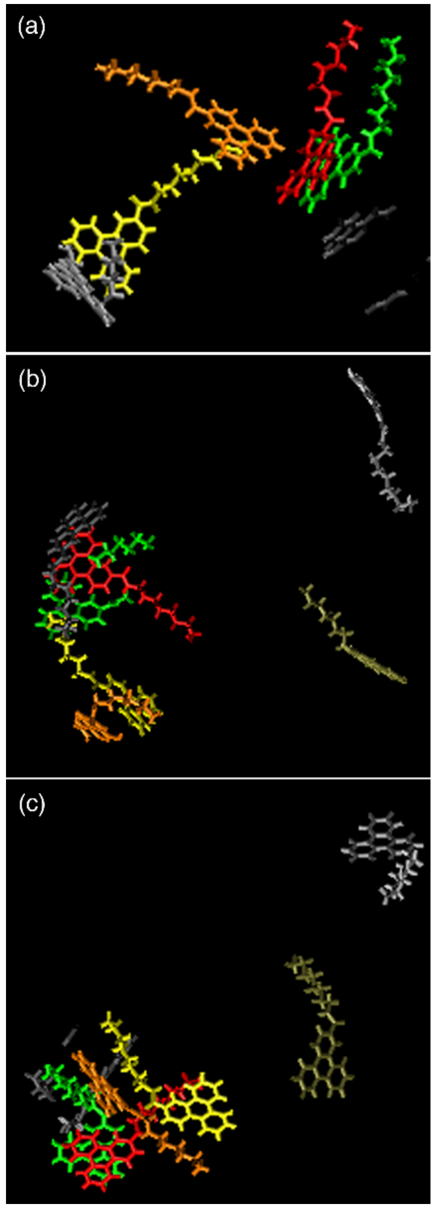

Figure 8. Snapshot of MD simulations of six molecules of TPN-CNAcid in toluene. Three possible configurations: (a) parallel stacking, (b) dissociation, and (c) non-parallel stacking, are observed in this set of images.

49x139mm (220 x 220 DPI)

Unable to Convert Image

The dimensions of this image (in pixels) are too large to be converted. For this image to convert, the total number of pixels (height x width) must be less than 40,000,000 (40 megapixels).

Figure 9. Calculated distances between the centers of mass for one molecule of model molecules of (a) TPN-C1 (repeated for context), (b) TPN-C3, (c) TPN-C5, and (d) TPN-C10, with the other 6 molecules present, during the 100 ns molecular dynamics simulation in toluene.